Mechanics and Mechanical Engineering
Vol. 13, No. 2 (2009) 5–21

Fracture of the Nonlinear Multi–Layered Composites

Mieczysław Jaroniek
Technical University of Łódź,
Department of Materials and Structures Strength
Stefanowskiego 1/15, 90-924 Łódź, Poland

Received (18 May 2009)
Revised (25 May 2009)
Accepted (20 Juli 2009)

Advanced mechanical and structural applications require accurate assessment of the damage state of materials during the fabrications as well as during the service. Due to the complex nature of the internal structure of the material, composites including the layered composite often fail in a variety of modes.

Fabrication of the functionally graded materials (FGM) can be obtained by layered mixing of two materials of different thermo–mechanical properties with different volume ratios gradually changed from layer to layer such that first layer has only a few particles of the other phase and last has maximum volume ratio of this other phase. The material (FGM) is functionally graded thermal and stress barrier.

Between the ceramic layer and metallic bond layer there exist a functionally graded layer "2" that contains volume of the bond (metallic) phase as a function of the distance y from he bond layer and volume ratio of the ceramics phase also as a function of y distance from the bond layer.

The failure modes very often are influenced by the local material properties that may develop in time under heat and pressure, local defect distribution, process induced residual stress, and other factors.

Fracture problems in the layer can be studied using J integral in finite element method, because it is not path independent

Consider a laminate composite in plane stress conditions, multi–layered beam bonded to planes. The fracture mechanics problem will be analysed using the photoelastic visualisation of the fracture events in a model structure

Keywords: Composites, multi–layered beams, fracture mechanic, photoelastic method, finite element method

1. Introduction

Fabrication of the model of the FGM can be obtained by layered mixing of two photoelastic materials of different thermo-mechanical properties with different volume ratios gradually changed from layer to layer such that first layer has only a few particles of the other phase and last has maximum volume ratio of this other phase.

The development of the failure criterion for a particular application is also very important for the predictions of the crack path and critical loads.

Recently, there has been a successful attempt to formulate problems of multiple cracks without any limitation. This attempt was concluded with the series of papers summarising the undertaken research for isotropic [2], anisotropy [4] and non–homogeneous class of problems [5] and [4].

Crack propagation in multi–layered composites of finite thickness is especially challenging and open field for investigation. Some results have been recently reported in [5]. The numerical calculations were carried out using the finite element programs ANSYS 9 and 10 [11]. Two different methods were used: solid modeling and direct generation.

2. Material properties

Material properties exert an influence on the stress distribution and concentration, damage process and load carrying capacity of elements. In the case of elastic–plastic materials, a region of plastic strains originates in most heavily loaded cross–sections. In order to visualise the state of strains and stresses, some tests have been performed on the samples made of an "araldite"–type optically active epoxy resin (Ep–53), modified with softening agents in such a way that an elastic material has been obtained. Properties of the components of experimental model are given in Tab. 1.

Table 1 Mechanical properties of the experimental model components

Layer	Young's Modulus $\mathbf{E}_i$ [MPa]	Poisson's ratio ν_i [1]	Photoelastic constants in terms of stresses k_σ [MPa/fr]	Photoelastic constants in terms of strain f_ε [-/fr]
1	3450.0	0.35	1.68	$6.572 \cdot 10^{-4}$
2	1705.0	0.36	1.18	$9.412 \cdot 10^{-4}$
3	821.0	0.38	0.855	$14.31 \cdot 10^{-4}$
4	683.0	0.40	0.819	$16.79 \cdot 10^{-4}$

3. Experimental Results

The stress distribution in was determined using two methods:

Shear Stress Difference Procedure (SDP – evaluation a complete stress state by means the isochromatics and the angles of the isoclines along the cuts) [3].

Method of the characteristics (the stress distribution were determined using the isochromatics only and the equations of equilibrium [10].

In a general case [7], the Cartesian components of stress: σ_x , σ_y and τ_{xy} in the neighbourhood of the crack tip are:

$$\begin{aligned} \sigma_x &= \frac{K_I}{\sqrt{2\pi r}} \cos\frac{\Theta}{2}\left(1 - \sin\frac{\Theta}{2}\sin\frac{3\Theta}{2}\right) + \sigma_{ox} \\ \sigma_y &= \frac{K_I}{\sqrt{2\pi r}} \cos\frac{\Theta}{2}\left(1 + \sin\frac{\Theta}{2}\sin\frac{3\Theta}{2}\right) \\ \tau_{xy} &= \frac{1}{\sqrt{2\pi r}}\left[K_I \sin\frac{\Theta}{2}\cos\frac{\Theta}{2}\cos\frac{3\Theta}{2}\right) + K_{II}\cos\frac{\Theta}{2}\left(1 - \sin\frac{\Theta}{2}\sin\frac{2\Theta}{2}\right)] \end{aligned} \tag{1}$$

From which:

$$(\sigma_1-\sigma_2)^2=\frac{1}{2\pi r}\left[(K_I\sin\Theta+2K_{II}\cos\Theta)^2+(K_{II}\sin\Theta)^2\right]$$
$$-2\frac{\sigma_{ox}}{\sqrt{2\pi r}}\sin\frac{\Theta}{2}\left[K_I\sin\Theta(1+2\cos\Theta)+K_{II}(1+2\cos^2\Theta+\cos\Theta)\right]+\sigma_{ox}^2 \tag{2}$$

where K_I and K_{II} are the stress–intensity factors, r and θ are coordinates of a polar coordinate system.

By inserting the values $k_\sigma m_i=\sigma_1-\sigma_2$ into (2) we obtain the isochromatics curves in polar coordinates $(r,\ \Theta)$. For each isochromatic loop the position of maximum angle Θ_m corresponds to the maximum radius of the r_m. This principle can also be used in the mixed mode analysis [7] by employing information from two loops in the near field of the crack, if the far field stress component – $\sigma_{ox}(\Theta)=\text{const}$. Differentiating Eqn (2) with respect to Θ, setting $\Theta=\Theta_m$ and $r=r_m$ and using equation $\partial\tau_m/\partial\Theta_m=0$ gives:

$$\begin{aligned}
&g(K_I,K_{II},\sigma_{ox})=\frac{1}{2\pi r}\left[K_I^2\sin2\Theta+4K_IK_{II}\cos2\Theta-3K_{II}^2\sin2\Theta\right]\\
&-2\frac{\sigma_{ox}}{\sqrt{2\pi rr}}\sin\frac{\Theta}{2}\left\{\ [K_I(\cos\Theta+2\cos2\Theta)-K_{II}(2\sin2\Theta+\sin\Theta)]\right.\\
&\left.+\frac{1}{2}\cos\frac{\Theta}{2}\left[K_i(\sin\Theta+\sin2\Theta)+K_{II}(2+\cos2\Theta+\cos\Theta)\right]\ \right\}\\
&f(K_I,K_{II},\sigma_{ox})=(\sigma_1-\sigma_2)^2-(k_\sigma m)^2=0\\
&g(K_I,K_{II},\sigma_{ox})=\frac{\partial[(\sigma_1-\sigma_2)^2]}{\partial\Theta_m}=0
\end{aligned} \tag{3}$$

Substituting the radii r_m and the angles Θ_m from these two loops into a pair of equations of the form given in Eqn (3) gives two independent relations dependent on the parameters K_I, K_{II} and σ_{ox}. The third equation is obtained by using (2). The three equations obtained in this way have the form

$$\begin{aligned}
g_i(K_I,K_{II},\sigma_{ox}) &= 0\\
g_j(K_I,K_{II},\sigma_{ox}) &= 0\\
f_k(K_I,K_{II},\sigma_{ox}) &= 0
\end{aligned} \tag{4}$$

In order to determine K_I, K_{II} and σ_{ox} it is sufficient to select two arbitrary points r_i, Θ_i and apply the Newton–Raphson method to the solution of three simultaneous non–linear equations (4).

The values K_C according to mixed mode of the fracture were obtained from

$$K_C=\sqrt{K_I^2+K_{II}^2} \tag{5}$$

Example of the numerical results obtained from (4):

$m=12.5$, $r_1=0.6$ mm, $\Theta_1=1.484$, $r_2=10.45$ mm, $\Theta_2=1.416$,
$K_I^{(4)}=0.14$ MPa$\sqrt{\text{m}}$, $K_{II}^{(4)}=1.05$ MPa$\sqrt{\text{m}}$, $\sigma_{ox}=0.039$ MPa,
$K_C^{(4)}=1.05$ MPa$\sqrt{\text{m}}$

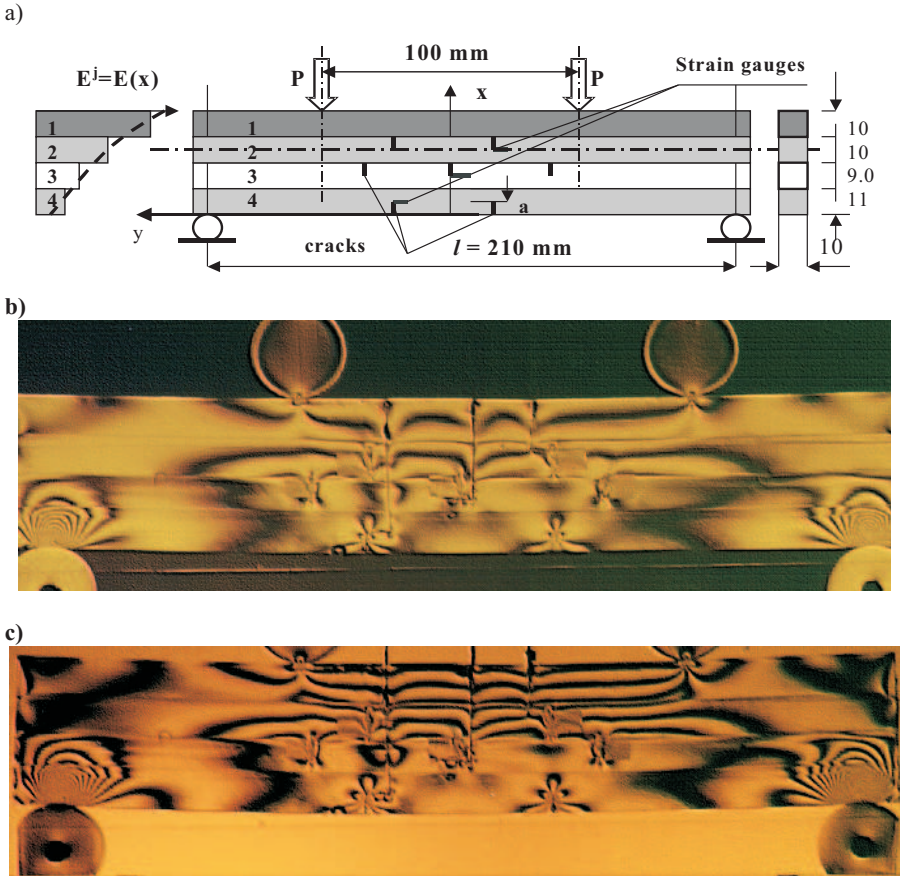

Figure 1 a) Four–layer beam with cracks. Photoelastic model under four point bending, the isochromatic patterns ($\sigma_1 - \sigma_2$) distribution b) Initial loading (P=20.0 N) c) P=50.0 N - tension of layers 2, 3 and 4

By inserting the values r_i, Θ_i in three selected arbitrary points into (2) we obtain three non–linear equations (i = 1, 2, 3)

$$f_i(K_I, K_{II}, \sigma_{ox}) = 0 \tag{6}$$

and apply the Newton–Raphson method to the solution we have K_I, K_{II} and σ_{ox}. Example of the numerical results (shown in Fig. 3) obtained from (6) for:

$m_1 = 12.5$, $r_1 = 0.72$ mm, $\Theta_1 = 1.484$, $m_2 = 8.0$,
$r_2 = 1.15$ mm, $\Theta_2 = 1.37$, $m_3 = 5.5$ mm, $r_3 = 1.85$,
$\Theta_3 = 1.315$, $K_I^{(4)} = 0.702$ MPa$\sqrt{\text{m}}$, $K_{II}^{(4)} = 1.043$ MPa$\sqrt{\text{m}}$,
$\sigma_{ox} = 0.152$ Mpa, $K_C^{(4)} = 1.257$ MPa$\sqrt{\text{m}}$

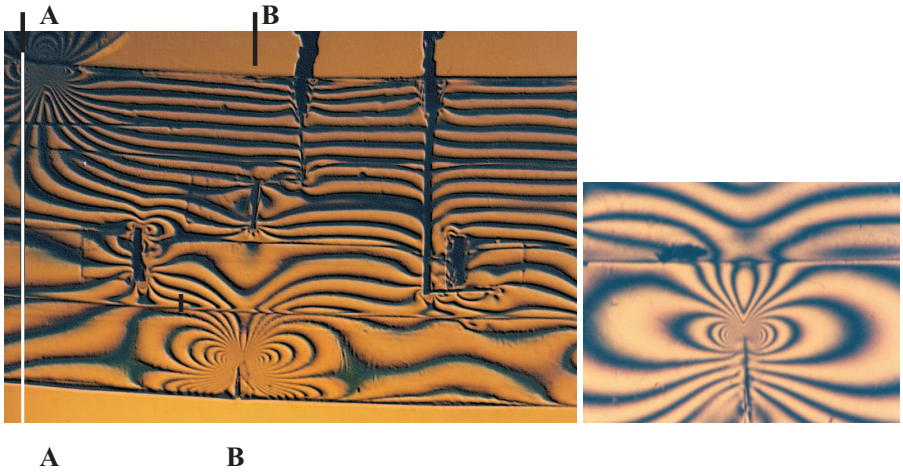

Figure 2 The isochromatic patterns $(\sigma_1 - \sigma_2)$ distribution according to the propagation of the crack obtained experimentally

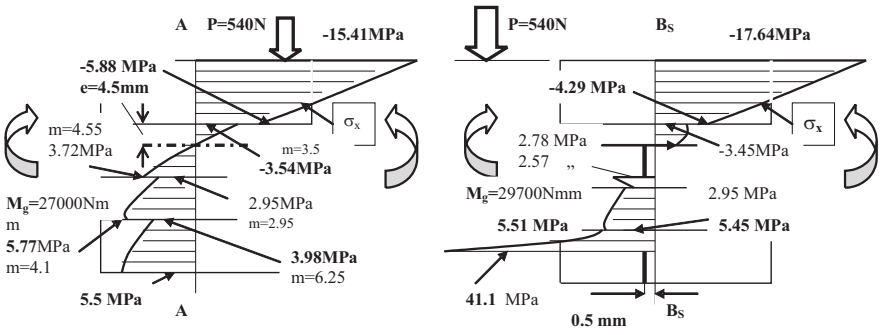

Figure 3 Distribution of stresses in cros sections A-A and B-B 0.5mm with respect to crack obtained experimentally

4. The stress analysis from complex potentials

In the present paper the elastic and plastic deformation has been approximately analysed using the Muskhelishvili's complex potentials method.

$$\sigma_{xx} + \sigma_{yy} = 4\mathrm{Re}\left[\psi'(z)\right]$$
$$\sigma_{yy} - \sigma_{xx} + 2i\tau_{xy} = 2\left[\bar{z}\psi''(z) + \chi''(z)\right]$$
$$2G(u + iv) = \kappa\psi(z) - z\bar{\psi}'(\bar{z}) - \bar{\chi}'(\bar{z})$$
$$2G(u' + iv') = \kappa\psi'(z) - z\bar{\psi}'(\bar{z}) - z\overline{\psi"(z)} - \bar{\chi}"(\bar{z})$$

where $\kappa = 3 - 4\nu$ for plain strain and $\kappa = \frac{3-\nu}{1+\nu}$ plain stress

$$\begin{aligned}
&\sigma_{xx} + \sigma_{yy} = 4\mathrm{Re}\left[\psi'(z)\right] \\
&\sigma_{yy} - \sigma_{xx} = \mathrm{Re}2\left[\bar{z}\psi''(z) + \chi''(z)\right] \\
&\tau_{xy} = \mathrm{Im}\left[\bar{z}\psi''(z) + \chi''(z)\right]
\end{aligned}$$

The elastostatic stress field is required to satisfy the well–known equilibrium equations [1] using two analytic functions $\psi(z)$ and $\chi(z)$

$$\begin{aligned}
&\sigma_{xx} = \mathrm{Re}\left[2\psi'(z) - \bar{z}\psi''(z) - \chi''(z)\right] \\
&\sigma_{yy} = \mathrm{Re}\left[2\psi'(z) + \bar{z}\psi''(z) + \chi''(z)\right] \\
&\tau_{xy} = \mathrm{Im}\left[\bar{z}\psi''(z) + \chi''(z)\right] \\
&2G(u + i\upsilon) = \kappa\psi(z) - z\bar{\psi}'(z) - \bar{\chi}'(z) \\
&\chi''(z) = -z\psi''(z)
\end{aligned} \tag{7}$$

Using two analytic functions $\psi(z)$ and $\chi(z)$

$$\psi'(z) = \psi_1'(z) + \psi_2'(z) \qquad \chi''(z) = z\left[\psi_1''(z) - \psi_2''(z)\right]$$

The complex stress potentials are assumed as follows

$$\begin{aligned}
2\psi^j(z) &= \sum_{n=1}^{N}\left[C_n \int z^{(2-n)}\sqrt{\frac{z-a}{z+a}}dz\right] \\
2\psi'^{(j)}(z) &= \sum_{n=1}^{N}\sqrt{\frac{z-a}{z+a}}C_n^j z^{(2-n)} \\
2\psi_2(z) &= \sum_{n=1}^{N}\left[D_n \int \frac{z^{(3-n)}dz}{\sqrt{z^2-a^2}}\right] \\
2\psi_2'(z) &= \sum_{n=1}^{N}\left[\frac{D_n z^{(3-n)}}{\sqrt{z^2-a^2}}\right]
\end{aligned} \tag{8}$$

The stress σ_x , σ_y and τ_{xy} characterizes by

$$\begin{aligned}
&\sigma_x = \mathrm{Re}\left[2\psi' - 2x\psi_1''\right] - y\mathrm{Im}2\psi_2'' \\
&\sigma_y = \mathrm{Re}\left[2\psi' + 2x\psi_1''\right] + y\mathrm{Im}2\psi_2'' \\
&\tau_{xy} = x\mathrm{Im}2\psi_1'' - y\mathrm{Re}2\psi_2''
\end{aligned}$$

The stress–intensity factors are related by:

$$\begin{aligned}
&K_I = \lim_{\substack{x\to a \\ a}} \sigma_y(x,0)\sqrt{2\pi(x-a)} \qquad && K_I = \lim_{x\to a} \sigma_y(x,0)\sqrt{2\pi(x-a)} \\
&K_{II} = \lim_{\substack{x\to a \\ a}} \tau_{xy}(x,0)\sqrt{2\pi(x-a)} && K_{II} = \lim_{\substack{x\to a \\ a}} \tau_{xy}(x,0)\sqrt{2\pi(x-a)} \\
&G_C = 2\int_0^a p(x)u_y(x,0)\,dx && G_C = 2\int_0^a p(x)u_y(x,0)\,dx
\end{aligned} \tag{9}$$

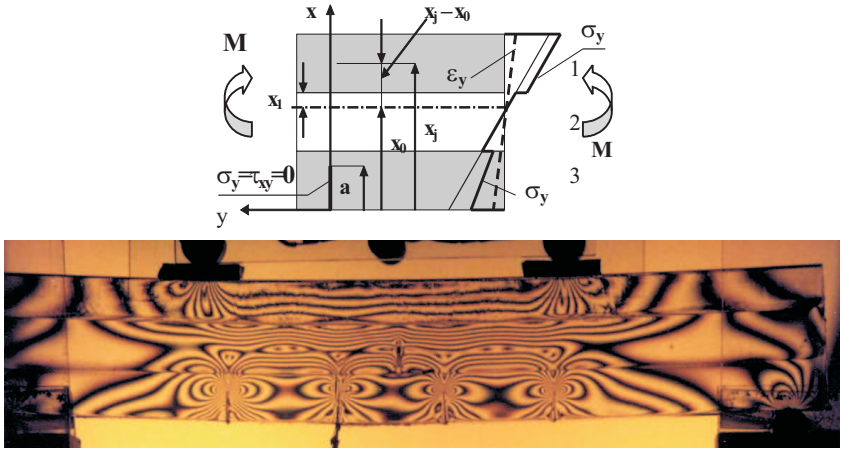

Figure 4 The boundary conditions for 3 layer beam and isochromatic patterns $(\sigma_1 - \sigma_2)$ distribution corresponding to vertical crack

By inserting the (8) into (9) we obtain

$$K_I^{(j)} = \lim_{x \to a} \left\{ \mathrm{Re}\left[2\psi'^{(j)}(z) \right] + x 2\psi''^{(j)}(z) \right\} \sqrt{2\pi (x-a)}$$
$$K_{II}^{(j)} = \lim_{x \to a} \left\{ x \mathrm{Im}\left[2\psi'^{(j)}(z) \right] \right\} \sqrt{2\pi (x-a)}$$

and

$$\begin{aligned}
\sigma_x^j &= \sum_{n=1}^{N} \left\{ \mathrm{Re}\left[(\overline{C}_n^j + i\overline{\overline{C}}_n^j) f_1(z) + (\overline{D}_n^j + i\overline{\overline{D}}_n^j) f_2(z) \right] \right\} \\
&\quad - \sum_{n=1}^{N} \left\{ y \mathrm{Im}\left[(\overline{D}_n^j + i\overline{\overline{D}}_n^j) f_3(z) \right] \right\} \\
\sigma_y^j &= \sum_{n=1}^{N} \left\{ \mathrm{Re}\left[(\overline{C}_n^j + i\overline{\overline{C}}_n^j) f_4(z) + (\overline{D}_n^j + i\overline{\overline{D}}_n^j) f_2(z) \right] \right\} \\
&\quad + \sum_{n=1}^{N} \left\{ y \mathrm{Im}\left[(\overline{D}_n^j + i\overline{\overline{D}}_n^j) f_3(z) \right] \right\}
\end{aligned} \tag{10}$$

$$\begin{aligned}
\tau_{xy}^j &= \sum_{n=1}^{N} \left\{ x \mathrm{Im}\left[(\overline{C}_n^j + i\overline{\overline{C}}_n^j) f_5(z) \right] \right\} \\
&\quad - \sum_{n=1}^{N} \left\{ y \mathrm{Re}\left[(\overline{D}_n^j + i\overline{\overline{D}}_n^j) f_3(z) \right] \right\}
\end{aligned}$$

For $y = 0$ in this case, the Cartesian components of stress: σ_x, σ_y and τ_{xy} are given as:

$$
\begin{aligned}
\sigma_x^j &= \sum_{n=1}^{N}\left\{\mathrm{Re}\left[(\overline{C}_n^j + i\overline{\overline{C}}_n^j) f_1(z)\right]\right\} \\
\sigma_y^j &= \sum_{n=1}^{N}\left\{\mathrm{Re}\left[(\overline{C}_n^j + i\overline{\overline{C}}_n^j) f_4(z)\right]\right\} \\
\tau_{xy}^j &= \sum_{n=1}^{N}\left\{x\mathrm{Im}\left[(\overline{C}_n^j + i\overline{\overline{C}}_n^j) f_5(z)\right]\right\} \\
f_1(z) &= \frac{1}{z^{n-1}}\left(\frac{1}{z}\sqrt{\frac{z-a}{z+a}} - x\frac{az-(n-2)(z^2-a^2)}{(z+a)\sqrt{z^2-a^2}}\right) \\
f_2(z) &= \frac{z^{3-n}}{\sqrt{z^2-a^2}} \\
f_3(z) &= z^{2-n}\frac{(3-n)(z^2-a^2)+z^2}{(z^2-a^2)^{3/2}} \\
f_4(z) &= \frac{1}{z^{n-1}}\left(\frac{1}{z}\sqrt{\frac{z-a}{z+a}} + x\frac{az-(n-2)(z^2-a^2)}{(z+a)\sqrt{z^2-a^2}}\right) \\
f_5(z) &= \frac{1}{z^{n-1}}\frac{az(n-2)(z^2-a^2)}{(z+a)\sqrt{z^2-a^2}}
\end{aligned}
\tag{11}
$$

$$
\begin{array}{ll}
C_n^i = \mathrm{Re}C_n^i + i\mathrm{Im}C_n^i & \overline{C_n^i} = \mathrm{Re}C_n^i \\
D_n^i = \mathrm{Re}D_n^i + i\mathrm{Im}D_n^i & \overline{\overline{C_n^i}} = \mathrm{Im}C_n^i
\end{array}
\tag{12}
$$

The boundary conditions can by expressed as

$$
\begin{array}{l}
\sigma_y^{(\infty)} - \sigma_x^{(\infty)} + 2i\tau_{xy}^{(\infty)} = (\overline{z}-z)\,2\psi\text{"}\,(z) + 2A \\
\sigma_g = -\dfrac{M}{I}(x-s) = \sigma_y^{\infty} \qquad \sigma_x^{\infty} = 0 \\
\dfrac{\varepsilon_y^j = \varepsilon_y^{j+1} \qquad \varepsilon_y^j = \partial v^j}{\partial y \qquad \varepsilon_x^j = \varepsilon_x^{j+1}} \\
u' = \dfrac{\partial u}{\partial x} \qquad u^j = u^{j+1} \qquad v^j = v^{j+1}
\end{array}
\tag{13}
$$

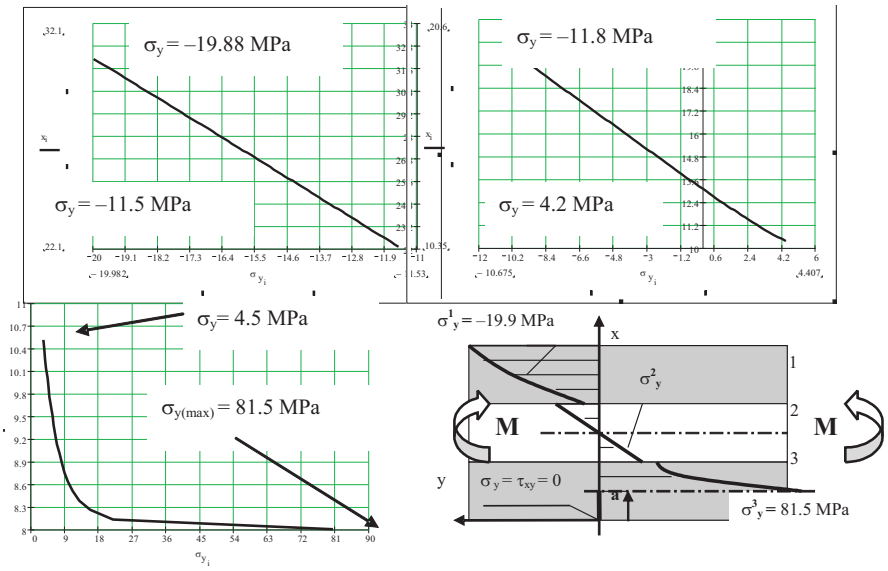

Figure 5 Distribution of stresses in cross sections A-A and B-B 0.5mm with respect to crack obtained experimentally and used in the analysis of the complex potentials

$$\int_0^H \sigma_y^j dx$$

$$= \sum_{n=1}^{N} \left\{ \mathrm{Re} \int_0^H \left[\frac{C_n^j}{z^{n-1}} \left(\frac{1}{z} \sqrt{\frac{z-a}{z+a}} + x \frac{az - (n-2)(z^2-a^2)}{(z+a)\sqrt{z^2-a^2}} \right) \right] dx \right\} = 0$$

$$\int_0^H b\sigma_y^j x dx + M \tag{14}$$

$$= \sum_{n=1}^{N} \left\{ \int_0^H b\mathrm{Re} \left[\frac{C_n^j}{z^{n-1}} \left(\frac{1}{z} \sqrt{\frac{z-a}{z+a}} + x \frac{az - (n-2)(z^2-a^2)}{(z+a)\sqrt{z^2-a^2}} \right) \right] dx \right\} + M = 0$$

$$\sigma_y^j = \sum_{n=1}^{N} \left\{ \mathrm{Re} \left[\frac{C_n^j}{z^{n-1}} \left(\frac{1}{z} \sqrt{\frac{z-a}{z+a}} + x \frac{az - (n-2)(z^2-a^2)}{(z+a)\sqrt{z^2-a^2}} \right) \right] \right\}$$

$$\sigma_g = -\frac{M}{I}(x-s) = \sigma_y^{\infty}$$

For each isochromatic loop $\sigma_1 - \sigma_2 = k_\sigma m$

$$\sigma_{yy} - \sigma_{xx} = k_\sigma m t \cos 2\alpha \tag{15}$$

in other hand $\sigma_1+\sigma_2=\sigma_{xx}+\sigma_{yy}$ and

$$\sigma_{xx}+\sigma_{yy}=\sum_{n=1}^{N}2\mathrm{Re}\left[C_n z^{(2-n)}\sqrt{\frac{z-a}{z+a}}+\frac{D_n z^{(3-n)}}{\sqrt{z^2-a^2}}\right] \tag{16}$$

This principle can be used in the analysis of the stresses, by inserting the values m_i, α_i in selected arbitrary points $P(r_i,\,\Theta_i)$ we obtain equations

$$\sum_{n=1}^{N}\left\{\mathrm{Re}\left[(\overline{C}_n+i\overline{\overline{C}}_n)[f_4(z)-f_1(z)]\right]+2y\mathrm{Im}\left[(\overline{D}_n+i\overline{\overline{D}}_n)f_3(z)\right]\right\}=k_\sigma m_i\cos 2\alpha_i$$

from which:

$$\begin{aligned}
K_{II}^{(j)} &= \lim_{x\to a}\sum_{n=1}^{N}\left\{x\mathrm{Im}\left[C_n^j f_4(z)\right]\sqrt{2\pi(x-a)}\right\} &(17)\\
K_{II}^{(j)} &= \lim_{x\to a}\sum_{n=1}^{N}\left\{x\mathrm{Im}\left[C_n^j f_5(z)\right]\sqrt{2\pi(x-a)}\right\}\\
\tau_m^2 &= \mathrm{Re}\left[\bar{z}\psi''(z)+\chi''(z)\right]^2+\mathrm{Im}\left[\bar{z}\psi''(z)+\chi''(z)\right]^2 &(18)\\
\tau_m^2 &= \left(\sum_{n=1}^{N}\left\{x\mathrm{Re}\left[C_n f_5(z)\right]+y\mathrm{Im}\left[D_n f_3(z)\right]\right\}\right)^2\\
&\quad+\left(\sum_{n=1}^{N}\left\{x\mathrm{Im}\left[C_n f_5(z)\right]-y\mathrm{Re}\left[D_n f_3(z)\right]\right\}\right)^2
\end{aligned}$$

For each isochromatic loop

$$\varepsilon_{yy}-\varepsilon_{xx}=\frac{1}{2G'}\sum_{n=1}^{N}\left\{\mathrm{Re}\left[(\overline{C}_n+i\overline{\overline{C}}_n)[f_4(z)-f_1(z)]\right]+2y\mathrm{Im}\left[(\overline{D}_n+i\overline{\overline{D}}_n)f_3(z)\right]\right\}$$

in other hand $\varepsilon_{yy}-\varepsilon_{xx}=f_\varepsilon(m)m\cos 2\alpha$ and

$$\begin{aligned}
&\frac{(1+\nu_j)}{E_j}\sum_{n=1}^{N}\left\{\mathrm{Re}\left[(\overline{C}_n^j+i\overline{\overline{C}}_n^j)[f_4(z)-f_1(z)]\right]+2y\mathrm{Im}\left[(\overline{D}_n^j+i\overline{\overline{D}}_n^j)f_3(z)\right]\right\}\\
&=f_\varepsilon m(x_t)\cos 2\alpha
\end{aligned}$$

$$\begin{aligned}
K_I &= \lim_{x\to a}\sum_{n=1}^{N}\left\{\mathrm{Re}\left[\frac{C_n}{z^{n-1}}\left(\frac{1}{z}\sqrt{\frac{z-a}{z+a}}+x\frac{az-(n-2)(z^2-a^2)}{(z+a)\sqrt{z^2-a^2}}\right)\right.\right.\\
&\quad\left.\left.+\frac{D_n z^{3-n}}{\sqrt{z^2-a^2}}\right]\sqrt{2\pi(x-a)}\right\} &(19)\\
K_{II} &= \lim_{x\to a}\sum_{n=1}^{N}\left\{x\mathrm{Im}\left[\frac{C_n}{z^{n-1}}\frac{az(n-2)(z^2-a^2)}{(z+a)\sqrt{z^2-a^2}}\right]\sqrt{2\pi(x-a)}\right\}
\end{aligned}$$

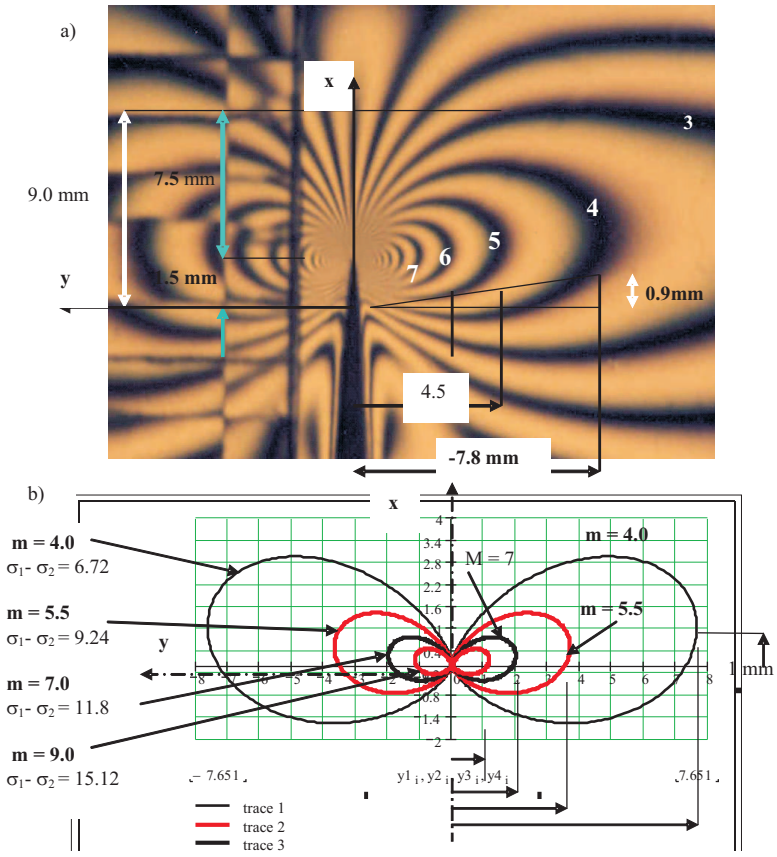

Figure 6 The isochromatic patterns $(\sigma_1 - \sigma_2)$ distribution according to the propagation of the crack obtained experimentally and used in the analysis of the complex potentials

Where

$$z^l\sqrt{\frac{z-a}{z+a}} = r^l\left(\frac{r_1}{r_2}\right)^{1/2}\left[\cos\left(\frac{\Theta_1+\Theta_2}{2}+\Theta l\right)+i\sin\left(\frac{\Theta_1+\Theta_2}{2}+\Theta l\right)\right]$$
$$\frac{z^l}{\sqrt{z^2-a^2}} = \frac{r^l}{(r_1r_2)^{1/2}}\left[\cos\left(\Theta l-\frac{\Theta_1+\Theta_2}{2}\right)+i\sin\left(\Theta l-\frac{\Theta_1+\Theta_2}{2}\right)\right]$$

Photoelastic measurements make possible deformations and stresses study in whole structure of elastomer. On basis of photoelastic measurements, we define directly difference of strains:

$$\begin{aligned}\sigma_1-\sigma_2 &= k_\delta m\\ \varepsilon_1-\varepsilon_2=\frac{1+\nu}{E}(\sigma_1-\sigma_2) &= \frac{1+\nu}{E}k_\delta m\end{aligned} \tag{20}$$

where:

$$f_\sigma = \frac{1+\nu}{E} k_\delta$$

$$f_\varepsilon = \frac{1+\nu}{E} k_\sigma$$

model constants corresponding to difference of stresses and main deformations.

As well as it is known lines for which differences between stresses and main strains have constant value and one color are called isochromatics. Next, basing on isochromatics measurements stresses distribution has been defined. Applying stress–strain relation, in elastic body deviator strain components are proportional to deviator stress component, as written:

$$\frac{\sigma_1 - \sigma_{sr}}{\varepsilon_1 - \varepsilon_{sr}} = \frac{\sigma_2 - \sigma_{sr}}{\varepsilon_2 - \varepsilon_{sr}} \tag{21}$$

Photoelastic measurements results one can apply also for strain and stress analyse concerning elasto–plastic materials. In elasto–plastic body, proportion of deviator strain components and deviator stress components is described by relation:

$$\frac{\sigma_1 - \sigma_{sr}}{\varepsilon_1 - \varepsilon_{sr}} = \frac{\sigma_2 - \sigma_{sr}}{\varepsilon_2 - \varepsilon_{sr}} = 2G' \tag{22}$$

where

$$G' = \frac{\tau_0}{\gamma_0} \left(\frac{\tau}{\gamma_0} \right)^{N-1}$$

$$\frac{E_s}{1+\nu_s} = \frac{2\frac{\sigma_o}{\varepsilon_o^p}\varepsilon^{p-1}}{3 - (1-2\nu_o)\left(\frac{\varepsilon}{\varepsilon_o}\right)^{p-1}}$$

$$\sigma_1 - \sigma_2 = \frac{2\frac{\sigma_o}{\varepsilon_o^p}\varepsilon^{p-1}}{3 - (1-2\nu_o)\left(\frac{\varepsilon}{\varepsilon_o}\right)^{p-1}} (\varepsilon_1 - \varepsilon_2)$$

$$\frac{\sigma_1 - \sigma_2}{\varepsilon_1 - \varepsilon_2} = \frac{2\frac{\sigma_o}{\varepsilon_o^p}\varepsilon^{p-1}}{3 - (1-2\nu_o)\left(\frac{\varepsilon}{\varepsilon_o}\right)^{p-1}}$$

For simply tensile test, when $\sigma_1 = \sigma$, $\sigma_2 = \sigma_3 = 0$, parameters $\varepsilon_1 = \varepsilon_{int}$, ε_2 and ε_3 one can determine on the basis of shape change low $\varepsilon_2 = \varepsilon_3 = -\frac{1}{2}(\varepsilon_{int} - 3\varepsilon_{sr})$, where $\sigma_{int} = \sigma = A\varepsilon^P$ and $\varepsilon_{int} = \left(\frac{1}{A}\sigma_{int}\right)^{1/p}$ or $\sigma_{sr} = \sigma/3$.

Main strains difference amount:

$$\varepsilon_1 - \varepsilon_2 = \tfrac{3}{2}\varepsilon_{int} - 3\varepsilon_{sr} \tag{23}$$

$$\varepsilon_1 - \varepsilon_2 = \frac{3}{2}\alpha_0\varepsilon_{pl}\left(\frac{J}{\alpha_0\sigma_{pl}\varepsilon_{pl}I_n}\right)^{\frac{n}{1+n}} r^{-\frac{n}{n+1}}\tilde{\sigma}_{int}^{n-1}\left[(\tilde{\sigma}_{rr} - \tilde{\sigma}_{\theta\theta})^2 - (2\tilde{\tau}_{r\theta})^2\right]^{1/2} \tag{24}$$

Where $\tilde{\sigma}_{int}^2 = \tilde{\sigma}_{rr}^2 + \tilde{\sigma}_{\theta\theta}^2 - \tilde{\sigma}_{rr}\tilde{\sigma}_{\theta\theta} + 3\tilde{\sigma}_{r\theta}^2$

$$\sigma_1 - \sigma_2 = \sigma_{pl}\left(\frac{J}{\alpha_0\sigma_{pl}\varepsilon_{pl}I_n}\right)^{\frac{1}{1+n}} r^{-\frac{1}{n+1}}\left[(\tilde{\sigma}_{rr} - \tilde{\sigma}_{\theta\theta})^2 - (2\tilde{\tau}_{r\theta})^2\right]^{1/2} \tag{25}$$

On basis of photoelastic measurements, we define directly difference of strains:

$$\begin{aligned} \sigma_1 - \sigma_2 &= k_\delta m \\ \varepsilon_1 - \varepsilon_2 &= \frac{1+\nu}{E}(\sigma_1 - \sigma_2) = \frac{1+\nu}{E} k_\delta m \end{aligned}$$

By inserting the values $\varepsilon_1 - \varepsilon_2$ into (24) we obtain the isochromatics curves in polar coordinates (r, Θ).

$$r_\varepsilon(\Theta) = \left(\frac{3}{2}\frac{\alpha_0 \varepsilon_{pl}}{f_\varepsilon m}\right)^{\frac{n+1}{n}} \left(\frac{J}{\alpha_0 \sigma_{pl} \varepsilon_{pl} I_n}\right) \tilde{\sigma}_{int}^{\frac{n^2-1}{n}} \left[(\tilde{\sigma}_{rr} - \tilde{\sigma}_{\theta\theta})^2 - (2\tilde{\tau}_{r\theta})^2\right]^{\frac{n+1}{2n}} \tag{26}$$

In elasto–plastic body, proportion of deviator strain components and deviator stress components is described by:

$$\frac{\sigma_1 - \sigma_2}{\varepsilon_1 - \varepsilon_2} = \frac{\sigma_{pl}}{\frac{3}{2}\alpha \varepsilon_{pl}} \left(\frac{J}{\alpha_0 \sigma_{pl} \varepsilon_{pl} I_n}\right)^{\frac{1-n}{1+n}} r^{-\frac{1-n}{n+1}} \tilde{\sigma}_{int}^{1-n} \tag{27}$$

5. Numerical determination of stress distribution

The distribution of stresses and displacements has been calculated using the finite element method (FEM) [11, 16]. Finite element calculations were performed in order to verify the experimentally observed the isochromatic distribution observe during cracks propagation. The geometry and materials of models were chosen to correspond to the actual specimens used in the experiments. The numerical calculations were carried out using the finite element program ANSYS 9 and by applying the substructure technique. A finite element mesh of the model (used for numerical simulation) are presented in Fig.7 and the stresses σ_x are shown in Fig. 9. For comparison the numerical (from FEM) and experimental isochromatic fringes ($\sigma_1 - \sigma_2$), distribution was shown in in Figs 8 and 10.

Table 2 Experimental and numerical results. Critical values $K_{IC}^{(1)}$ according to the propagation of the crack and $K_{IC}^{(2)}$

Crack length. a [mm]	Critical force P_{cr} [N]	Experimental res. [MPa$\sqrt{m}$]				Numerical res. [MPa$\sqrt{m}$]	
		$K_I^{(4)}$	$K_{II}^{(4)}$	$K_C^{(4)}$	σ_{ox} [MPa]	$G_C^{(4)}$ [MN/m]	$K_{C\,n}^{(4)}$ MPa$\sqrt{m}$
6.0	265.0	1.177	0.8793	**1.419**	2.58	3.08	**1.45**
9.0	205.0	0.702	1.043	**1.257**	0.152	2.39	**1.28**
9.8	185.0	0.14	1.05	**1.05**	0.039	1.97	**1.16**

Comparison between numerical and experimental results is presented in Figs. 8 and 10. The agreement between the finite element method predicted isochromatics–fringe patterns distribution and those determined photoelasticaly was found to be within 5 ÷8 percent.

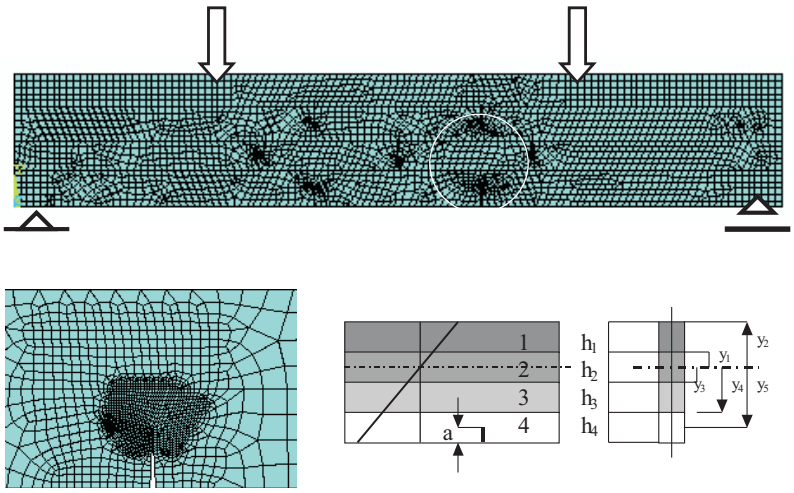

Figure 7 A finite element mesh of the model (for numerical simulation)

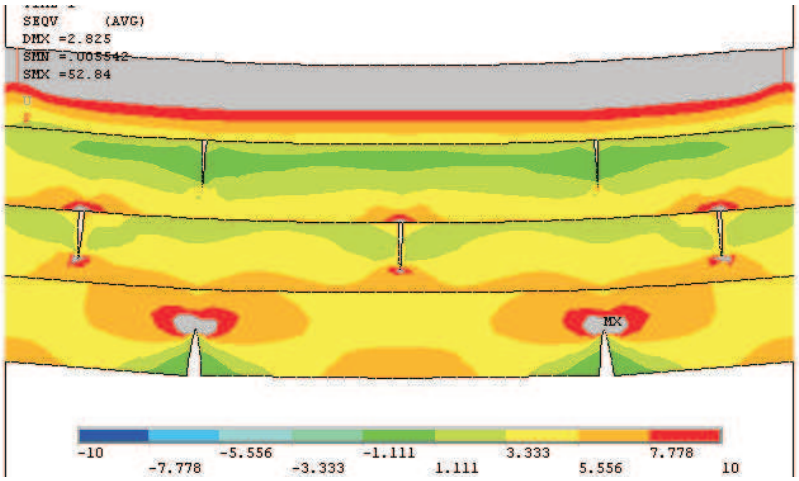

Figure 8 Numerical determination of stress distribution (Ansys 5.6). Distribution of the stresses σ_x (cracks length a=6.0 mm)

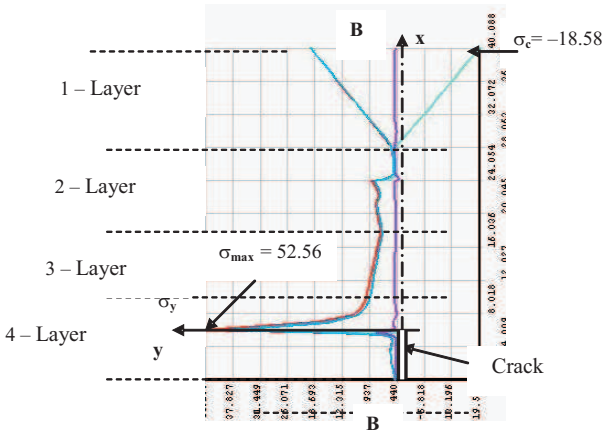

Figure 9 Numerical determination of stress distribution (Ansys 9). Distribution of the normal stress σ_x and equivalent stress σ_{int} along the crack

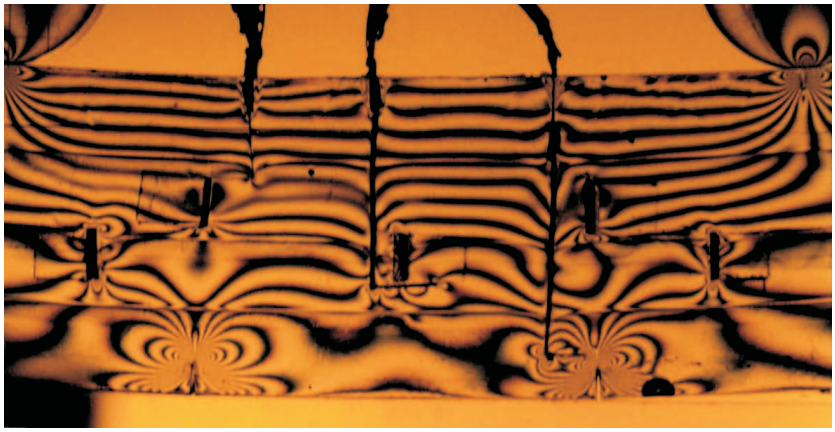

Figure 10 Experimental determination of stress distribution (The stress intensity). Distribution of the absolute values of $\sigma_1 - \sigma_2$ (cracks length a=6.0 mm)

6. Conclusions

Fabrication of the model of the FGM can be obtained similarly as the functionally graded materials by layered mixing of two photoelastic materials of different thermo–mechanical properties with different volume ratios gradually changed from layer to layer such that first layer has only a few particles of the other phase and last has maximum volume ratio of this other phase. Photoelasticity was shown to be promising in stress analysis of beams with various numbers and orientation of cracks.

In the present paper the elastic deformation has been approximately analysed using the Muskhelishvili's complex potentials method in the analysis of the stresses. Using two analytic functions in the analysis of the stresses we obtain equations for isochromatic loop.

The specimen can be build as layered beam, for example,

glass layer at the bottom then particles of the same glass in the epoxy in several layers of various volume ratio of the glass in epoxy and pure epoxy at the top.

The beam can be loaded in bending to generate cracks while will propagate through the FGM layer.

It is possible to fabricate a model using various photoelastic materials to model multi layered structure.

Finite element calculations (FEM) were performed in order to verify the experimentally observed branching phenomenon and the isochromatic distribution observed during cracks propagation. The agreement between the finite element method predicted isochromatics–fringe patterns distribution and those determined photoelasticaly was found to be within $3 \div 5$ percent.

References

[1] **Cherepanov G.P.**: Mechanics of brittle fracture, *Mc Graw – Hill*, New York, **1979**.

[2] **Cook T.S. and Erdogan F.**: Stresses in bonded materials with a crack perpendicular to the interface, *Int. Journ. of Engineering Science*, Vol. 10, 677–697, **1972**.

[3] **Frocht M.M.**: Photoelasticity, *John Wiley*, New York, **1960**.

[4] **Gupta A.G.**: Layered composite with a broken laminate, *International Journal of Solids and Structures*, No36 (1845-1864), **1973**.

[5] **Hilton P.D. and Sin G.C.**: A laminate composite with a crack normal to interfaces, *International Journal of Solids and Structures*, No 7, 913, **1971**.

[6] **Rychlewska J. and Woźniak C.**: Boundary layer phenomena in elastodynamics of functionally graded laminates, *Archives of Mechanics*, 58, 4–5, 431–444, **2006**.

[7] **Sanford R.J. and Dally J.**: A General Method For Determining Mixed–Mode Stress Intensity Factors From Isochromatic Fringe Patterns, —textitEng. Fract. Mech., Vol. 2, 621–633, **1979**.

[8] **Szczepiński W.**: A photoelastic method for determining stresses by means isochromes only, *Arch. of Applied Mechanics*, 5 (13), Warsaw, **1961**.

[9] **Szymczyk J. and Woźniak C.**: Continuum modelling of laminates with a slowly graded microstructure, *Archives of Mechanics*, 58, 4-5, 445–458, **2006**.

[10] **Theocaris P.S. and Gdoutos E.E.**: A photoelastic determination of K_I stress intensity factors, *Eng. Fract. Mech.*, Vol. 7, 331–339, **1975**.

[11] User's Guide ANSYS : Ansys 9, Inc., Huston, USA, **2006**.

[12] **Woźniak C.**: Nonlinear Macro–Elastodynamics of Microperiodic Composites, *Bull. Ac. Pol. Sci.: Tech. Sci.*, 41, 315–321, **1993**.

[13] **Woźniak C.**: Microdynamics: Continuum. Modelling the Simple Composite Materials, *J. Theor. Appl. Mech.*, 33, 267–289, **1995**.

[14] **Woźniak C.**: Nonlinear Macro–Elastodynamics of Microperiodic Composites, *Bull. Ac. Pol. Sei.: Tech. Sei.*, 41, 315–321, **1993**.

[15] **Woźniak C.**: Microdynamics: Continuum. Modelling the Simple Composite Materials, *J. Theor. Appl. Mech.*, 33, 267–289, **1995**.

[16] **Zienkiewicz O.C.**: The Finite Element Method in Engineering Science, *Mc Graw – Hill*, London, New York, **1971**.